Modeling and ZVS Constraints of the Hybrid LLC Resonant Converter for MHz Level Operation

Lingeshwaren Sobrayen, Patrick Dehem, Charif Karimi, Tanguy Phulpin, Daniel Sadarnac

Modeling and ZVS Constraints of the Hybrid LLC Resonant Converter for MHz Level Operation

Lingeshwaren Sobrayen*†‡, Patrick Dehem‡, Charif Karimi*†, Tanguy Phulpin*† and Daniel Sadarnac*†
*Université Paris-Saclay, CentraleSupélec, CNRS, Laboratoire de Génie Electrique et Electronique de Paris, 91192 Gif-sur-Yvette, France
†Sorbonne Université, CNRS, Laboratoire de Génie Electrique et Electronique de Paris, 75252 Paris, France
‡EnerSys S.A.R.L., Rue A. Fleming – Z.I. EST – CS40962, 62033 Arras, France

***Abstract*—This paper presents a model of the hybrid LLC converter, emphasizing on deadtime interval dynamics that become too impactful to ignore for preserving model accuracy at MHz-level operation. The time-domain modeling approach is adopted and a new parameter k_C, defined as the capacitance ratio between the resonant capacitance C_r and switch output capacitance C_{oss}, is introduced to model the state variables during the transition intervals. The proposed model, validated by PSIM circuit simulation, is used to derive ZVS constraints of the topology, especially for the less frequently addressed upper deadtime limit to prevent an eventual C_{oss} recharge, due to an early resonant current reversal. The ZVS limits proposed are validated on a 500W, 400V/18-36V GaN-based experimental prototype at 500kHz.**

I. Introduction

The LLC resonant converter [1] (Fig. 1(a)) is today a firmly established topology for high frequency dc-dc conversion due to simple circuit structure, capacitive output filter, full range soft switching ability, natural suitability for magnetic integration and low electromagnetic interference.

While the converter shows outstanding performance in narrow range designs such as DCX transformers for data-centre applications [2] where it operates close to its series resonant frequency f_r, in wide range applications such as PV microinverters, power supplies and battery chargers wherein a large switching frequency deviation from f_r is demanded, the performance of the converter rapidly degrades. Operation higher than f_r to reach a lower voltage conversion gain M puts higher stress on gate drivers, causes high turn-off device losses, entails ZCS loss of secondary side diodes along with associated reverse recovery issues, and confronts the converter to light load regulation problems due to the diode junction capacitances. Higher gain objectives, on the other side, calling for operation lower than f_r, leads to increasing circulating currents and a larger transformer core size that needs to be designed for the lowest switching frequency.

Amongst numerous solutions proposed to adapt the LLC converter for wide range applications [3], the hybrid LLC converter concept (Fig. 1(b)) introduced in [4] and developed in [5]–[7] shows remarkable effectiveness for $\times 2$ voltage conversion gains, with the addition of only two auxiliary switches to the LLC base topology. This gives the primary driving bridge the ability to alternate between a full-bridge and a half bridge within the same switching period, applying

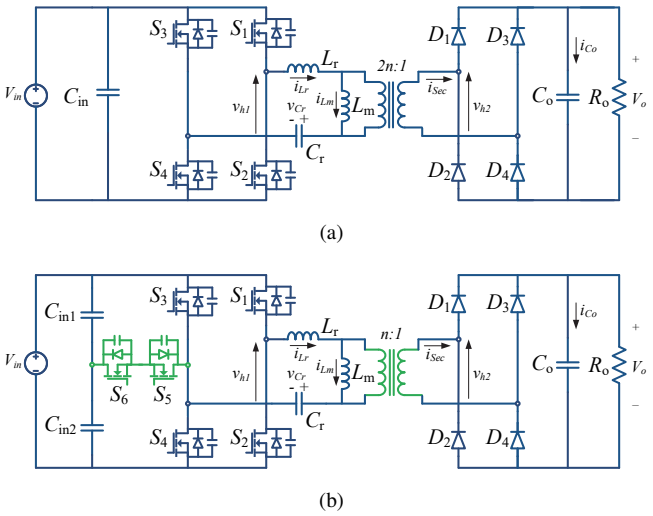

Fig. 1. (a) The LLC resonant converter, controlled by switching frequency variation (b) The hybrid LLC resonant converter, a resonant topology controlled by PWM at a fixed switching frequency

either V_{in} or $V_{in}/2$ to the resonant tank, as illustrated by the two-level step v_{h1} waveform in Fig. 2. Voltage regulation is realized at a fixed switching frequency by the duty cycle D control of the full-bridge usage over half a switching period. For $D = 0$ and $D = 1$ when a single voltage level is used, the resonant current i_{Lr} and magnetizing current i_{Lm} are purely sinusoidal and triangular respectively, while in between these two extreme operating points, the tank currents take the more general profiles also shown in Fig. 2, similar to a conventional LLC converter operating in the boost region, except for an additional segment in i_{Lr}.

While preserving the advantages of the LLC converter, the hybrid version features a step-down characteristic which halves the required transformer turns ratio, for the same input and output voltage specifications. A voltage conversion gain $M \in [1\ 2]$ for a regular LLC converter maps onto $M \in [0.5\ 1]$ for the hybrid LLC converter, a range which the converter can cover irrespective of the inductance ratio $k_L = L_m/L_r$ and the quality factor, Q of the resonant tank. With the magnetizing inductor L_m no longer relied upon for boosting action, higher values of k_L can be designed based solely on the ZVS constraints of primary active switches, which

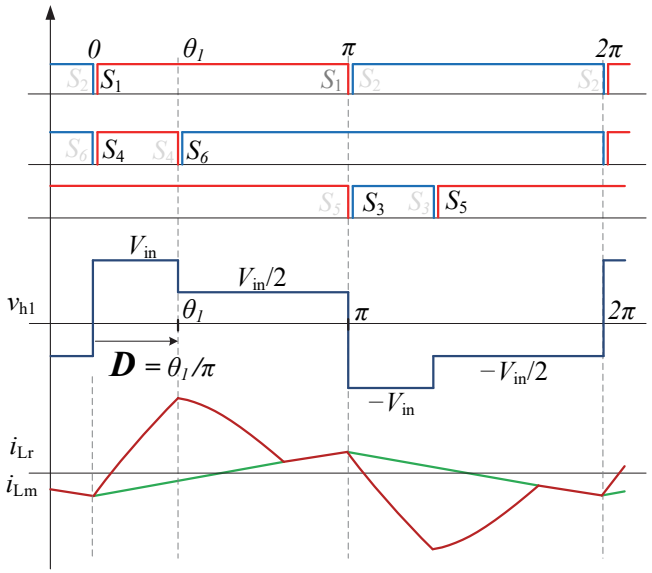

Fig. 2. Key waveforms of the hybrid LLC converter: Gating signals S_1-S_6, primary bridge voltage v_{h1}, resonant inductor current i_{Lr} and magnetizing inductor current i_{Lm}

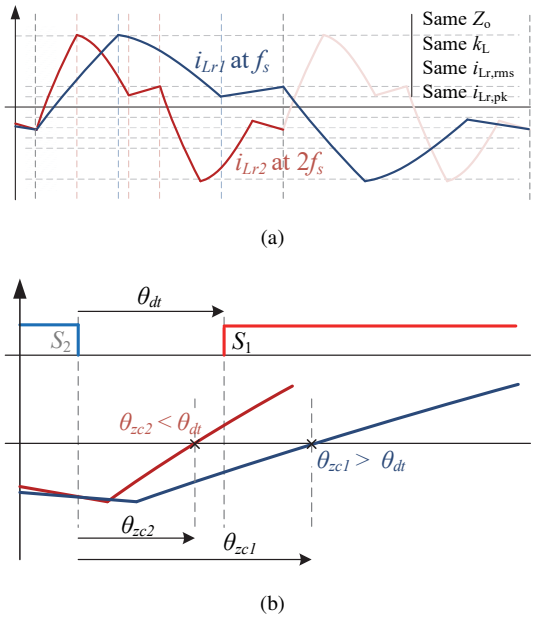

Fig. 3. (a) Typical resonant current waveform of frequencies f_s and $2f_s$ (b) Zoomed: zero crossings of f_s- and $2f_s$-resonant waveforms for same deadtime

combined with higher values of tank characteristic impedance $Z_o = \sqrt{L_r/C_r}$ leads to reduced rms currents in the converter.

Operation at fixed resonant frequency is particularly attractive for MHz level switching objectives, allowing the transformer, resonant tank, and filters all to be optimized at a single operating frequency across a $\times 2$ gain range. At high frequencies though, in this converter the set of values of Z_o and k_L that can cause a current reversal before the end of the deadtime interval is broader. This is illustrated in Fig. 3 with typical resonant tank current i_{Lr} waveforms of the converter for two frequencies: f_s and $2f_s$, with same Z_o and k_L designed values, for same peak and rms current levels. At higher frequency, there is more possibility for the zero crossing of i_{Lr} to occur before the gating signal of S_1 is applied if the deadtime is oversized, causing a recharge of its output capacitance and a missed opportunity for complete ZVS.

Deadtime intervals are generally reduced for higher frequency designs but even for GaN devices, manufacturers recommend a minimum limit of 50-100ns for 650V devices [8] with regards to driver delay skew and PCB stray inductances. For MHz-level operation, even a minimum of 50ns deadtime could be too long for an incorrectly designed resonant tank. An accurate model of the converter is hence important for proper design of the resonant tank and deadtime. The time-domain model proposed in [4], although significantly more precise than the first harmonic approximation (FHA) approach, ignores deadtime intervals in the analysis and therefore loses accuracy in the high frequency range, when the deadtime to switching period ratio becomes non-negligible. Some previous studies related to ZVS constraints at high frequency can be found in [9], [10] but they are applicable only to the conventional half-bridge LLC and use the less accurate FHA approach.

This paper presents an analysis that considers state variables evolution during transition intervals leading to a more accurate model for the hybrid LLC topology. The model can be used to predict the currents and voltages of interest even at high frequencies, based on which ZVS boundaries are derived to aid design and control. The paper is organized as follows: Section II describes the converter operation around half a switching period with deadtime dynamics and ZVS timing considerations explained. Section III presents the time-domain model of the converter and ZVS limits, verified in Section IV by simulation and in Section V experimentally.

II. Converter Operation

A. Modulation

The modulation scheme consists of three complementary switch pairs as shown in Fig. 2: $S_1(\overline{S_2})$, $S_3(\overline{S_5})$ and $S_4(\overline{S_6})$, controlled at a fixed switching frequency f_s, such that a two-level voltage waveform v_{h1} can be applied by the primary bridge to the resonant tank. S_1 and S_2 have a fixed duty ratio of 0.5. S_4 is controlled at a particular duty ratio and its rising edge is synchronized with that of S_1. S_4 conduction interval represents full-bridge mode of operation while its complementary switch S_6 conduction interval represents half-bridge mode of operation during a positive half cycle. Opposite phase complementary switches S_3 and S_5 are controlled in a similar fashion, synchronized with S_2 for conduction during the negative half period.

B. Normalization

Voltages, time, currents and frequency are normalized using the following bases: $V_{base} = V_{in}$, $t_{base} = \theta/\omega_r$, $I_{base} = V_{in}/Z_o$ and $f_{base} = f_r$, where V_{in} is the converter input

dc bus voltage, $\omega_r = 1/\sqrt{L_r C_r}$ is the resonant tank angular frequency, $Z_o = \sqrt{L_r/C_r}$ is the resonant tank characteristic impedance and $f_r = \omega_r/2\pi$ is the resonant tank frequency.

C. Circuit intervals

1) Interval 0^- ($t < t_0'$) [see Fig. 4(a) and Fig. 6]: Before t_0', the converter operates in half bridge mode, reaching the end of the negative half switching period, with switches S_2, S_5 and S_6 conducting. The converter is in LLC resonance, whereby the secondary side is disconnected from the primary side because of insufficient voltage developed across the magnetizing inductor voltage v_{Lm} to forward bias the output side diodes D_2 and D_3. L_m hence participates in resonance, and the resonant current i_{Lr}, equal to the magnetizing current i_{Lm}, is negative.

2) Interval 0 ($t_0' \leqslant t < t_0$) [see Fig. 4(b) and Fig. 6]: At t_0', switches S_2 and S_6 are turned off. Charges on the switch output capacitances $C_{oss1} - C_{oss6}$ of the switch network $S_1 - S_6$ start to redistribute themselves with the aid of the magnetizing current:
i) C_{oss1} starts discharging from V_{in} to 0; ii) C_{oss2} starts charging from 0 to V_{in}; iii) C_{oss3} starts charging from $V_{in}/2$ to V_{in}; iv) C_{oss4} starts discharging from $V_{in}/2$ to 0; v) C_{oss5} remains discharged as S_5 is kept on; vi) C_{oss6} starts charging from 0 to $V_{in}/2$. The primary bridge voltage v_{h1} starts inverting its polarity from $-V_{in}/2$ to V_{in} and the magnetizing inductor L_m, part of a resonant tank being subjected to a linearly increasing excitation voltage v_{h1}, sees its voltage v_{Lm} rising as well.

3) Interval 1 ($t_0 \leqslant t < t_1$) [see Fig. 5(a) and Fig. 6]: At t_0, v_{Lm} reaches the reflected output voltage nV_o, forward biasing diodes D_1 and D_4 to re-establish connection of the circuit's secondary. The normalized time duration from S_2/S_6 turn-off and L_m leaving resonance and getting clamped to nV_o is defined as the clamping time θ_{clamp}. A further time interval ($\alpha_1 < \theta < \alpha_3$) as shown in the v_{Lm} axis of Fig. 6(b) is required to fully discharge output capacitances of incoming switches S_1 and S_4, defined as the discharge time θ_{disch}. From this instant, body diodes of both S_1 and S_4 conduct the negative resonant current which marks the onset of the window of opportunity for full ZVS that ends at $\theta = \alpha_5$ at the zero current crossing of i_{Lr}; this interval is defined as the zero current crossing duration θ_{zc}. The normalized resonant inductor current i_{Lr}, resonant capacitor voltage v_{Cr}, magnetizing current i_{Lm} and magnetizing voltage v_{Lm} are given by

$$\begin{aligned} i_{Lr}(\theta) &= i_{Lr}(0)\cos\theta + [1 - M - v_{Cr}(0)]\sin\theta && \text{(1a)}\\ v_{Cr}(\theta) &= 1 - M - [1 - M - v_{Cr}(0)]\cos\theta \\ &\quad + i_{Lr}(0)\sin\theta && \text{(1b)}\\ i_{Lm}(\theta) &= i_{Lr}(0) + M\theta/k_L && \text{(1c)}\\ v_{Lm}(\theta) &= M && \text{(1d)} \end{aligned}$$

where $M = nV_o/V_{in}$ is the normalized output voltage or conversion gain of the converter. A small approximation is made at the beginning of the interval whereby the resonant tank input voltage v_{h1} is assumed to have already reached its final voltage of V_{in} as from $\theta = \alpha_1$ instead of slightly later at $\theta = \alpha_3$.

4) Interval 2 ($t_1 \leqslant t < t_2$) [see Fig. 5(b) and Fig. 6(a)]: At $t = t_1$, gating signal of S_4 is removed. Charges of switch output capacitances $C_{oss3} - C_{oss6}$ of the T-type leg start to redistribute themselves with the aid of the positive resonant tank current: 1) C_{oss3} starts discharging from V_{in} to $V_{in}/2$; 2) C_{oss4} starts charging from 0 to $V_{in}/2$; 3) C_{oss5} is unaffected and remains uncharged as S_5 is kept on; 4) C_{oss6} starts discharging from $V_{in}/2$ to 0. Its body diode starts conducting hereafter, preparing for its ZVS turn-on. The resonant tank normalized currents and voltages are now given by

$$\begin{aligned} i_{Lr}(\theta) &= [1 + (1/3)k_C] i_{Lr}(\theta_1)\cos(\theta - \theta_1) \\ &\quad + [1 - M - v_{Cr}(\theta_1)]\sin(\theta - \theta_1) \\ &\quad - (1/3)k_C i_{Lr}(\theta - \theta_1) && \text{(2a)}\\ v_{Cr}(\theta) &= 1 - [1 - M - v_{Cr}(\theta_1)]\cos(\theta - \theta_1) \\ &\quad + [1 + (1/3)k_C] i_{Lr}(\theta_1)\sin(\theta - \theta_1) \\ &\quad - (1/3)k_C i_{Lr}(\theta - \theta_1) && \text{(2b)}\\ i_{Lm}(\theta) &= i_{Lr}(0) + M\theta/k_L && \text{(2c)}\\ v_{Lm}(\theta) &= M && \text{(2d)} \end{aligned}$$

where k_C is the resonant capacitance to switch output capacitance ratio is given by

$$k_C = \frac{C_r}{C_{oss}} \tag{3}$$

A charge equivalent C_{oss} is assumed for the three active capacitances to model their $V_{in}/2$ voltage swings, driven by the positive resonant current $i_{Lr}(\theta_1)$ considered constant during this very short interval.

This interval marks the end of operation in full-bridge mode at $\theta = \theta_2$, based on which the duty ratio of the converter is defined as $D = \theta_2/\pi \approx \theta_1/\pi$.

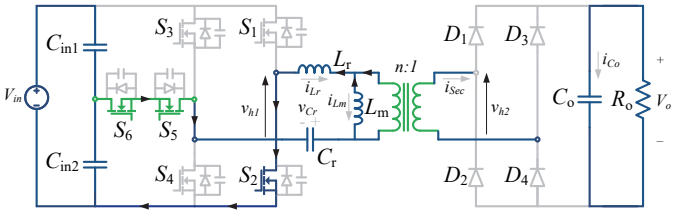

(a) Interval 0: $t < t_0'$

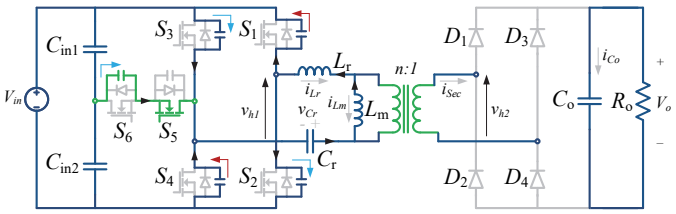

(b) Interval 0^-: $t_0' \leqslant t < t_0$

Fig. 4. Pre-analysis converter equivalent switching states transitioning from a negative to a positive half cycle

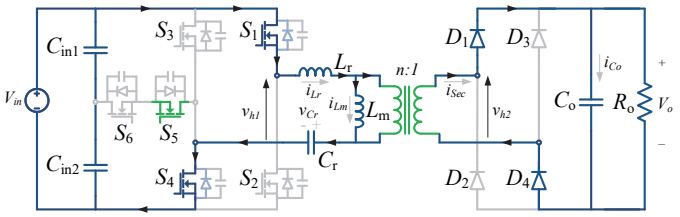

(a) Interval I: $t_0 \leqslant t < t_1$

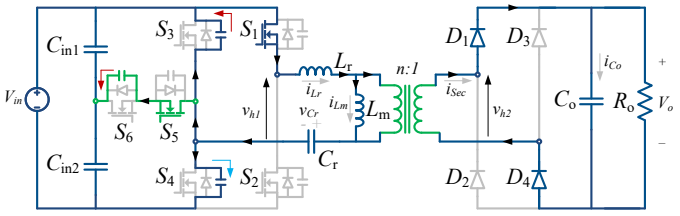

(b) Interval II: $t_1 \leqslant t < t_2$

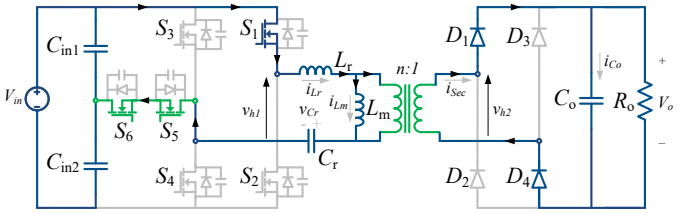

(c) Interval III: $t_2 \leqslant t < t_3$

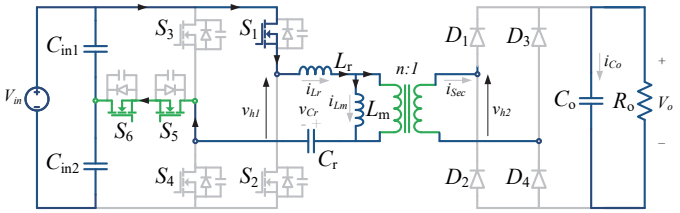

(d) Interval IV: $t_3 \leqslant t < t_4$

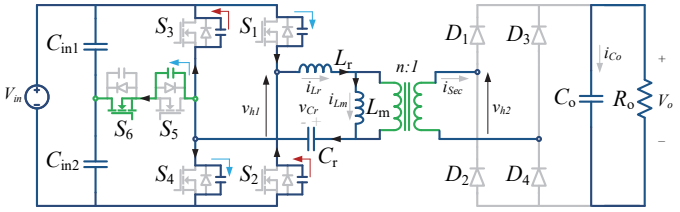

(e) Interval V: $t_4 \leqslant t < t_5$

Fig. 5. Converter equivalent switching states during a positive half cycle

5) Interval 3 ($t_2 \leqslant t < t_3$) [see Fig. 5(c) and Fig. 6(a)]: At $t = t_2$, gating signal of S_6 is applied and turns on under ZVS; current flowing in its body diode is transferred to the MOSFET channel that starts conducting in synchronous rectification mode. The converter operates in half-bridge mode, with the resonant tank being excited by half of the dc bus voltage. The resonant tank normalized currents and voltages are now given by

$$i_{\mathrm{Lr}}(\theta) = i_{\mathrm{Lr}}(\theta_2)\cos(\theta-\theta_2) + [0.5 - M - v_{\mathrm{Cr}}(\theta_2)]\sin(\theta-\theta_2) \quad (4a)$$

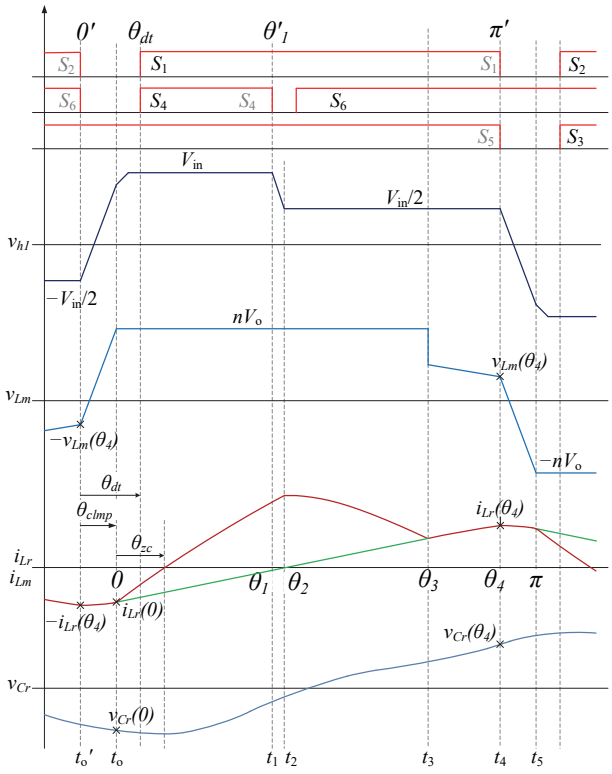

(a)

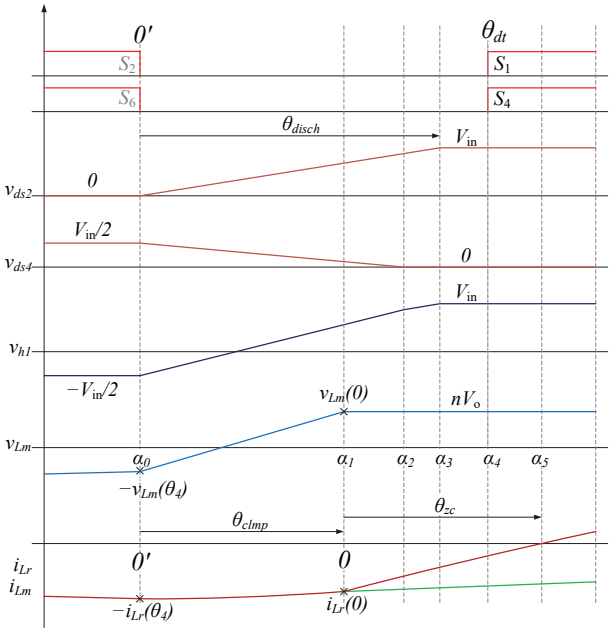

(b)

Fig. 6. (a) Converter modulation signals and waveforms around a positive half cycle and (b) Zoomed: voltage and current transitions during deadtime period $0' \leqslant \theta < \theta_{\mathrm{dt}}$

$$v_{\mathrm{Cr}}(\theta) = 0.5 - M - [0.5 - M - v_{\mathrm{Cr}}(\theta_2)]\cos(\theta-\theta_2) + i_{\mathrm{Lr}}(\theta_2)\sin(\theta-\theta_2) \quad (4b)$$

$$i_{\mathrm{Lm}}(\theta) = i_{\mathrm{Lr}}(0) + M\theta/k_{\mathrm{L}} \quad (4c)$$

$$v_{\mathrm{Lm}}(\theta) = M \tag{4d}$$

6) Interval 4 ($t_3 \leqslant t < t_4$) [see Fig. 5(d) and Fig. 6(a)]: At $t = t_3$, the resonant current i_{Lr} becomes equal to the magnetizing current i_{Lm}, which marks the transition from LC resonance to LLC resonance, with the circuit's secondary getting disconnected from the primary. This circuit interval is symmetrical to interval 0^-. The resonant tank normalized currents and voltages given by:

$$\begin{aligned}
i_{\mathrm{Lr}}(\theta) &= i_{\mathrm{Lr}}(\theta_3)k'_{\mathrm{L}}\cos(k'_{\mathrm{L}}(\theta-\theta_3)) \\
&\quad +[0.5-v_{\mathrm{Cr}}(\theta_3)]k'_{\mathrm{L}}\sin(k'_{\mathrm{L}}(\theta-\theta_3)) && \text{(5a)}\\
v_{\mathrm{Cr}}(\theta) &= 0.5-[0.5-v_{\mathrm{Cr}}(\theta_3)]\cos(k'_{\mathrm{L}}(\theta-\theta_3)) \\
&\quad +(1/k'_{\mathrm{L}})i_{\mathrm{Lr}}(\theta_3)\sin(k'_{\mathrm{L}}(\theta-\theta_3)) && \text{(5b)}\\
i_{\mathrm{Lm}}(\theta) &= i_{\mathrm{Lr}}(\theta) && \text{(5c)}\\
v_{\mathrm{Lm}}(\theta) &= [k_{\mathrm{L}}/(k_{\mathrm{L}}+1]\{[0.5-v_{\mathrm{Cr}}(\theta_3)]\cos(k'_{\mathrm{L}}(\theta-\theta_3)) \\
&\quad -i_{\mathrm{Lr}}(\theta_3)(1/k'_{\mathrm{L}})\sin(k'_{\mathrm{L}}(\theta-\theta_3))\} && \text{(5d)}
\end{aligned}$$

where $k'_{\mathrm{L}} = 1/\sqrt{1+k_{\mathrm{L}}}$

7) Interval 5 ($t_4 \leqslant t < t_5$) [see Fig. 5(e) and Fig. 6(a)]: At t_4, switches S_1 and S_5 are turned off. Charges on the switch output capacitances $C_{\mathrm{oss1}}-C_{\mathrm{oss6}}$ of the switch network S_1-S_6 start to redistribute themselves with the aid of the magnetizing current:
i) C_{oss1} starts charging from 0 to V_{in}; ii) C_{oss2} starts discharging from V_{in} to 0; iii) C_{oss3} starts discharging from $V_{\mathrm{in}}/2$ to 0; iv) C_{oss4} starts charging from $V_{\mathrm{in}}/2$ to V_{in}; vi) C_{oss5} starts charging from 0 to $V_{\mathrm{in}}/2$. vi) C_{oss6} remains discharged as S_6 is kept on; The primary bridge voltage v_{h1} starts inverting its polarity from $V_{\mathrm{in}}/2$ to $-V_{\mathrm{in}}$ and the magnetizing inductor L_{m}, part of a resonant tank being subjected to a linearly decreasing excitation voltage v_{h1}, sees its voltage v_{Lm} falling as well. This interval is symmetrical to interval 0. The resonant tank normalized currents and voltages given by:

$$\begin{aligned}
i_{\mathrm{Lr}}(\theta) &= (1+(5/6)k_{\mathrm{C}})i_{\mathrm{Lr}}(\theta_4)\cos(k'_{\mathrm{L}}(\theta-\theta_4)) \\
&\quad +[0.5-v_{\mathrm{Cr}}(\theta_4)]k'_{\mathrm{L}}\sin(k'_{\mathrm{L}}(\theta-\theta_4)) \\
&\quad -(5/6)k_{\mathrm{C}}i_{\mathrm{Lr}}(\theta-\theta_4) && \text{(6a)}\\
v_{\mathrm{Cr}}(\theta) &= 0.5-[0.5-v_{\mathrm{Cr}}(\theta_4)]\cos(\theta-\theta_4) \\
&\quad +(1+(5/6)k_{\mathrm{C}})i_{\mathrm{Lr}}(\theta_4)(1/k'_{\mathrm{L}})\sin(k'_{\mathrm{L}}(\theta-\theta_4)) \\
&\quad -(5/6)k_{\mathrm{C}}i_{\mathrm{Lr}}(\theta-\theta_4) && \text{(6b)}\\
i_{\mathrm{Lm}}(\theta) &= i_{\mathrm{Lr}}(\theta) && \text{(6c)}\\
v_{\mathrm{Lm}}(\theta) &= [k_{\mathrm{L}}/(k_{\mathrm{L}}+1]\{[0.5-v_{\mathrm{Cr}}(\theta_4)]\cos(k'_{\mathrm{L}}(\theta-\theta_4)) \\
&\quad -(1+(5/6)k_{\mathrm{C}})i_{\mathrm{Lr}}(\theta_4)(1/k'_{\mathrm{L}}) \\
&\quad \cdot\sin(k'_{\mathrm{L}}(\theta-\theta_4))\} && \text{(6d)}
\end{aligned}$$

The magnetizing current responsible for charging and discharging the capacitances of the switch network is considered constant at $i_{\mathrm{Lr}}(\theta_4)$ during this interval – this is a fair assumption especially in the case of the hybrid LLC converter where the $L_{\mathrm{m}}/L_{\mathrm{r}}$ ratio is high.

III. Model Derivation

By imposing continuity conditions on the resonant tank quantities i_{Lr}, v_{Cr} and i_{Lm} described by the piecewise nonlinear segments $(1)-(6)$, intermediate variables can be eliminated to advance to a model of the converter. To simplify the formulation, the minor deadtime interval $t_1 \leqslant t < t_2$ allowed for full bridge to half bridge transition is neglected – this as opposed to the major deadtime interval $t_4 \leqslant t < t_5$ that sees a voltage swing of $3V_{\mathrm{in}}/2$ in v_{h1}, sees only a $V_{\mathrm{in}}/2$ change. This smaller voltage movement is moreover ensured by the peak resonant current which allows a quick transition compared to the major deadtime interval that involves the magnetizing current purposefully kept low for minimizing turn-off losses.

$$\begin{aligned}
&i_{\mathrm{Lr}}(0)+i_{\mathrm{Lr}}(\theta_4)\cos(k'_{\mathrm{L}}(\pi-\theta_4))+[0.5-v_{\mathrm{Cr}}(\theta_4)]k'_{\mathrm{L}}\sin(k'_{\mathrm{L}}(\pi-\theta_4)) \\
&\qquad +(5/6)i_{\mathrm{Lr}}(\theta_4)k_{\mathrm{C}}[\cos(k'_{\mathrm{L}}(\pi-\theta_4))-1]=0 && \text{(9a)}\\
&v_{\mathrm{Cr}}(0)+0.5-[0.5-v_{\mathrm{Cr}}(\theta_4)]\cos(k'_{\mathrm{L}}(\pi-\theta_4))+i_{\mathrm{Lr}}(\theta_4)(1/k'_{\mathrm{L}})\sin(k'_{\mathrm{L}}(\pi-\theta_4)) \\
&\qquad +(5/6)i_{\mathrm{Lr}}(\theta_4)k_{\mathrm{C}}[(1/k'_{\mathrm{L}})\sin(k'_{\mathrm{L}}(\pi-\theta_4))-(\pi-\theta_4)]=0 && \text{(9b)}\\
&M+[k_{\mathrm{L}}/(k_{\mathrm{L}}+1)]\{[0.5-v_{\mathrm{Cr}}(\theta_4)]\cos(k'_{\mathrm{L}}(\pi-\theta_4))+i_{\mathrm{Lr}}(\theta_4)(1/k'_{\mathrm{L}})\sin(k'_{\mathrm{L}}(\pi-\theta_4)) \\
&\qquad +(5/6)i_{\mathrm{Lr}}(\theta_4)k_{\mathrm{C}}[(1/k'_{\mathrm{L}})\sin(k'_{\mathrm{L}}(\pi-\theta_4))\}=0 && \text{(9c)}\\
&i_{\mathrm{Lr}}(\theta_4)-\cos(k'_{\mathrm{L}}(\theta_4-\theta_3))[i_{\mathrm{Lr}}(0)\cos\theta_3+(1-M-v_{\mathrm{Cr}}(0))\sin\theta_3-0.5\sin(\theta_3-\theta_1)]-k'_{\mathrm{L}}\sin(k'_{\mathrm{L}}(\theta_4-\theta_3)) \\
&\qquad [M-0.5\cos(\theta_3-\theta_1)+(1-M-v_{\mathrm{Cr}}(0))\cos\theta_3-i_{\mathrm{Lr}}(0)\sin\theta_3]=0 && \text{(9d)}\\
&v_{\mathrm{Cr}}(\theta_4)-0.5+\cos(k'_{\mathrm{L}}(\theta_4-\theta_3))[M-0.5\cos(\theta_3-\theta_1)+(1-M-v_{\mathrm{Cr}}(0))\cos\theta_3-i_{\mathrm{Lr}}(0)\sin\theta_3] \\
&\qquad -(1/k'_{\mathrm{L}})\sin(k'_{\mathrm{L}}(\theta_4-\theta_3))[(1-M-v_{\mathrm{Cr}}(0))\sin\theta_3-0.5\sin(\theta_3-\theta_1)]=0 && \text{(9e)}\\
&i_{\mathrm{Lr}}(0)(\cos\theta_3-1)+[1-M-v_{\mathrm{Cr}}(0)]\sin\theta_3-0.5\sin(\theta_3-\theta_1)-M\theta_3/k_{\mathrm{L}}=0 && \text{(9f)}\\
&[1-M-v_{\mathrm{Cr}}(0)](1-\cos\theta_3)+0.5[\cos(\theta_3-\theta_1)-1]+i_{\mathrm{Lr}}(0)[\sin\theta_3-\theta_3]-M\theta_3^2/2k_{\mathrm{L}}-8MQ/\pi=0 && \text{(9g)}
\end{aligned}$$

Formulation

Based on the development of the resonant tank state variables from (1)-(4), and applying half-wave symmetry condition

$$i_{\mathrm{Lr}}(\pi) = -i_{\mathrm{Lr}}(0) \tag{7a}$$
$$v_{\mathrm{Cr}}(\pi) = -v_{\mathrm{Cr}}(0) \tag{7b}$$

tank currents equivalence at $\theta = \theta_3$

$$i_{\mathrm{Lr}}(\theta_3) = i_{\mathrm{Lm}}(\theta_3) \tag{7c}$$

magnetizing inductor voltage clamping at half period

$$v_{\mathrm{Lm}}(\pi) = -M \tag{7d}$$

power transfer equivalence over half period

$$\frac{1}{\pi}\int_0^{\pi} \left(i_{\mathrm{Lr}}(\theta) - i_{\mathrm{Lm}}(\theta)\right) d\theta = I_o = \frac{8MQ}{\pi^2} \tag{7e}$$

where the quality factor Q is given by

$$Q = \frac{\pi^2 Z_{\mathrm{o}}}{8n^2 R_{\mathrm{o}}} = \frac{\pi^2}{8}\frac{I_{\mathrm{o}}}{V_{\mathrm{o}}}\frac{1}{n^2}Z_{\mathrm{o}} = \frac{\pi^2}{8}\frac{P_{\mathrm{o}}}{(nV_{\mathrm{o}})^2}Z_{\mathrm{o}} \tag{8}$$

the time domain model of the converter can be derived as as in (1).

ZVS constraints

Based on the model, deadtime boundaries for ZVS realization are derived as in (3):

$$\theta_{\mathrm{disch}} < \theta_{\mathrm{dt}} < \theta_{\mathrm{clamp}} + \theta_{\mathrm{zc}} \tag{9a}$$

where

$$\theta_{\mathrm{disch}} = 2\frac{i_{\mathrm{Lr}}(\theta_4)}{k_{\mathrm{C}}} \tag{9b}$$
$$\theta_{\mathrm{clamp}} = \pi - \theta_4 \tag{9c}$$
$$\theta_{\mathrm{zc}} = \tan^{-1}\left[\frac{i_{\mathrm{Lr}}(0)}{1 - M - v_{\mathrm{Cr}}(0)}\right] \tag{9d}$$

The lower limit relates to the complete discharge of output capacitances of incoming switches and the upper limit avoids their recharge due to an early resonant current reversal.

IV. Model validation by simulation

The accuracy of the proposed model is validated against PSIM simulation of a hybrid LLC converter for $V_{\mathrm{in}} = 400$V, $V_{\mathrm{o}} = 18-36$V, $P_{\mathrm{o}} = 1$kW and $f_{\mathrm{s}} = 1$MHz. Circuit parameters

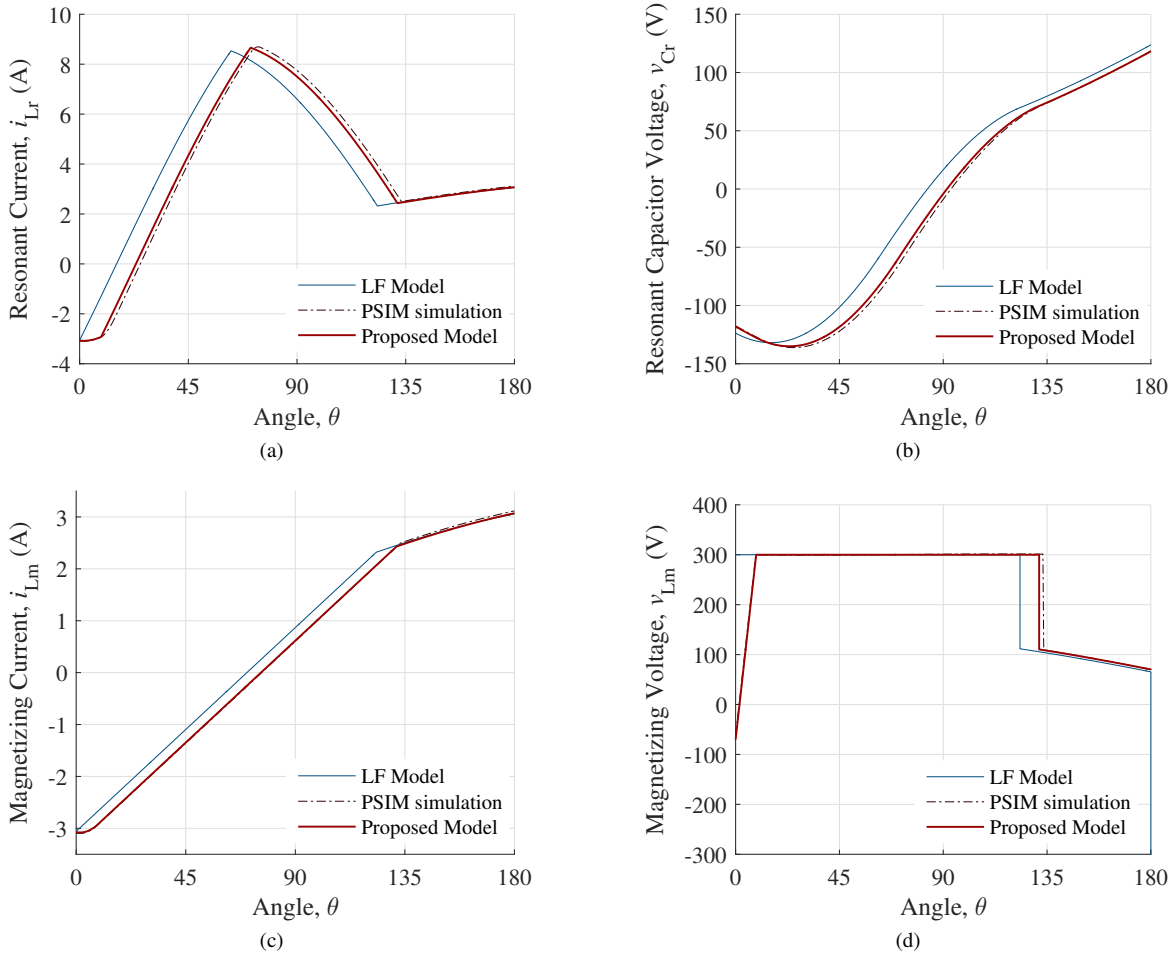

Fig. 7. Comparison of resonant tank quantities model predictions compared with PSIM simulations and LF model in [4] over half switching period for (a) resonant current i_{Lr} (b) resonant voltage v_{Cr} (c) magnetizing current i_{Lm} and (d) magnetizing voltage v_{Lm}

are as follow: $L_\mathrm{r} = 3.18\mu$H, $L_\mathrm{m} = 22.3\mu$H, $C_\mathrm{r} = 7.96$nF, $C_\mathrm{oss} = 150$pF, $Z_\mathrm{o} = 20\Omega$, $k_\mathrm{L} = 6$, $k_\mathrm{C} = 18.8$, $n = 11.1$.

The circuit is simulated at a fixed 1-ns time step and allowed to reach steady-state before results of the resonant current, resonant capacitor voltage, magnetizing current and magnetizing voltage are exported into MATLAB for benchmarking. Datapoints over half a cycle for i_h1, v_Cr, i_Lm and v_Lm are plotted in Fig. 7 at $V_\mathrm{o} = 27$V. For further comparison, the model proposed in [4] herein referred to as a low frequency (LF) model is also solved and plotted for the same design parameters and operating point. It can be observed that the LF model shows poor accuracy at this frequency level, whereas the proposed model is able to track simulation curves fairly accurately. The model shows equally good agreement with simulation results across the entire output voltage range and load range. The small discrepancy that exists are due to some simplifying assumptions made to preserve model simplicity. These assumptions could be either addressed for a perfect model fit, but for all practical design purposes, the presented model is sufficiently accurate.

V. Experimental Validation

The ZVS limits derived from the proposed model, are verified on a 400V/18-36V GaN-based prototype at 500kHz/500W. The primary bridge is built with GS66506T GaN HEMTs, that based on experimental measurements, show a lumped equivalent C_oss of 210pF for a 400V v_ds swing, that also takes into account the PCB stray and transformer interwinding capacitances. Circuit parameters are as follow: $L_\mathrm{r} = 9.2\mu$H, $L_\mathrm{m} = 72.6\mu$H, $C_\mathrm{r} = 11$nF, $C_\mathrm{oss} = 210$pF, $f_\mathrm{r} = 500$kHz, $Z_\mathrm{o} = 28.9\Omega$, $k_\mathrm{L} = 7.9$, $k_\mathrm{C} = 52.4$, $n = 11.1$.

Experimental waveforms for gating signals v_gs1 and v_gs2 of switches S_1 and S_2 respectively, S_1 drain-to-source voltage v_ds1, and resonant current i_Lr are shown in Fig. 8, to illustrate full ZVS realization attempts of S_1 for three deadtime design cases. When t_dead = 80ns (Fig. 8(a)), the discharge of the S_1 output capacitance is incomplete causing a quasi-ZVS situation that contributes to switching losses, gate ringing, EMI and in some extreme cases cause a gate failure if the 10V maximum v_gs absolute rating is crossed due to a subotptimally laid out GaN PCB. On the other hand if t_dead is oversized at 180ns (Fig. 8(b)), after the zero crossing of i_Lr at 150ns, the reverse current recharges back the output capacitance of S_1 and the full ZVS opportunity is lost, causing the same issues associated with a partial ZVS. Finally if t_dead = 120ns (Fig. 8(c)), the output capacitance of S_1 is completely discharged and the resonant current is comfortably above zero before its gating signal is applied.

At this operating point and the design parameters, the model predicts a C_oss discharge time of 106ns and an i_Lr zero current crossing time of 140ns, compared to measured times of 110ns and 150ns respectively.

VI. Conclusion

A time-domain model of the recently proposed hybrid LLC resonant converter is presented, where the major deadtime interval dynamics that become impactful at high frequencies are considered. The model shows good agreement with circuit simulation data in terms of key characterizing waveforms of the topology as well as in predicting the switch C_oss discharge, magnetizing inductor clamping, and zero-current crossing times. ZVS constraints relying on these quantities,

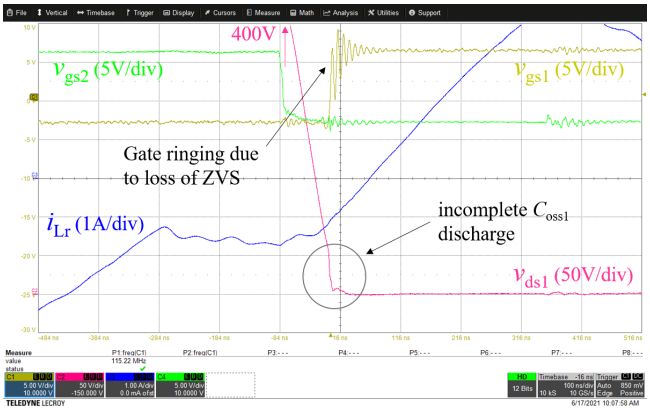

(a)

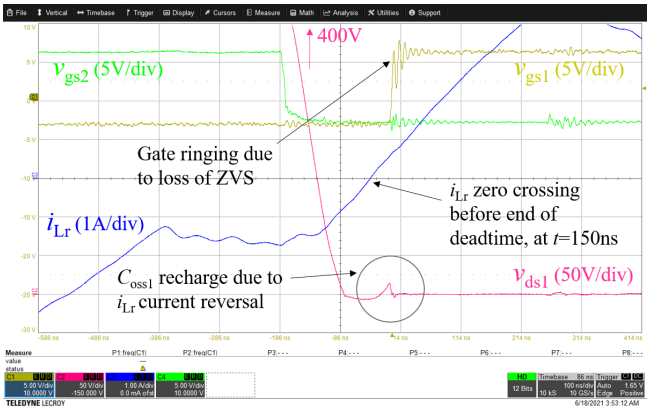

(b)

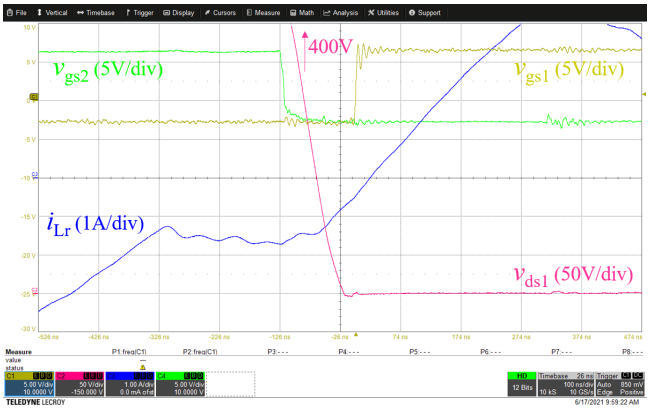

(c)

Fig. 8. Oscillographs of ZVS attempts made on a 500kHz/500W GaN prototype at V_in = 400V, P_o = 500W and V_o = 27V – for three deadtime design cases (a) incomplete ZVS due to insufficient time allowed for C_oss1 discharge (b) missed complete ZVS opportunity due to early current reversal and (c) complete ZVS realization with t_dead within ZVS boundaries of proposed model

are experimentally verified on a 500kHz/500W GaN prototype. The model proposed can be further improved by factoring in non-linear C_{oss} effects and other circuit parasitic elements, but in light of the experimental runs conducted, is deemed a right balance between model complexity/solvability and useful ZVS predictions.

REFERENCES

[1] B. Yang, F. C. Lee, A. Zhang, and G. Huang, "Llc resonant converter for front end dc/dc conversion," in *APEC. Seventeenth Annual IEEE Applied Power Electronics Conference and Exposition (Cat. No. 02CH37335)*, vol. 2, pp. 1108–1112. IEEE, 2002.

[2] M. H. Ahmed, M. A. de Rooij, and J. Wang, "High-power density, 900-w llc converters for servers using gan fets: Toward greater efficiency and power density in 48 v to 6\/12 v converters," *IEEE Power Electronics Magazine*, vol. 6, no. 1, pp. 40–47, 2019.

[3] Q. Cao, Z. Li, and H. Wang, "Wide voltage gain range llc dc/dc topologies: State-of-the-art," in *2018 International Power Electronics Conference (IPEC-Niigata 2018-ECCE Asia)*, pp. 100–107. IEEE, 2018.

[4] X. Sun, X. Li, Y. Shen, B. Wang, and X. Guo, "Dual-bridge llc resonant converter with fixed-frequency pwm control for wide input applications," *IEEE Transactions on Power Electronics*, vol. 32, no. 1, pp. 69–80, 2016.

[5] Y. Shen, H. Wang, A. Al-Durra, Z. Qin, and F. Blaabjerg, "A structure-reconfigurable series resonant dc–dc converter with wide-input and configurable-output voltages," *IEEE Transactions on Industry Applications*, vol. 55, no. 2, pp. 1752–1764, 2018.

[6] Y. Shen, H. Wang, A. Al-Durra, Z. Qin, and F. Blaabjerg, "A bidirectional resonant dc–dc converter suitable for wide voltage gain range," *IEEE Transactions on Power Electronics*, vol. 33, no. 4, pp. 2957–2975, 2017.

[7] Y. Shen, H. Wang, Z. Shen, Y. Yang, and F. Blaabjerg, "A 1-mhz series resonant dc–dc converter with a dual-mode rectifier for pv microinverters," *IEEE Transactions on Power Electronics*, vol. 34, no. 7, pp. 6544–6564, 2018.

[8] G. A. Guide, "Design with gan enhancement mode hemt," *GaN Systems Inc., Ottawa, Ontario, Canada, Apr*, vol. 12, 2018.

[9] R. Ren, B. Liu, E. A. Jones, F. Wang, Z. Zhang, and D. Costinett, "Accurate zvs boundary in high switching frequency llc converter," in *2016 IEEE Energy Conversion Congress and Exposition (ECCE)*, pp. 1–6. IEEE, 2016.

[10] W. Qin, L. Zhang, and X. Wu, "Re-examination of zvs condition for mhz llc converter operating at resonant frequency," in *2018 IEEE International Power Electronics and Application Conference and Exposition (PEAC)*, pp. 1–4. IEEE, 2018.